Nano Energy 60 (2019) 661–666

Contents lists available at ScienceDirect

Nano Energy

journal homepage: www.elsevier.com/locate/nanoen

Full paper

Breaking the symmetry: Gradient in NiFe layered double hydroxide nanoarrays for efficient oxygen evolution

Daojin Zhou[a,b,1], Yin Jia[a,c,1], Xinxuan Duan[a,c], Jialun Tang[d], Jie Xu[e], Dong Liu[b], Xuya Xiong[a], Junming Zhang[b], Jun Luo[e], Lirong Zheng[f], Bin Liu[b,**], Yun Kuang[a,***], Xiaoming Sun[a,c,*], Xue Duan[a]

[a] State Key Laboratory of Chemical Resource Engineering, Beijing Advanced Innovation Center for Soft Matter Science and Engineering, Beijing University of Chemical Technology, Beijing, 100029, China
[b] School of Chemical and Biomedical Engineering, Nanyang Technological University, Singapore, 637459, Singapore
[c] College of Energy, Beijing University of Chemical Technology, Beijing, 100029, China
[d] Beijing Key Laboratory of Nanophotonics and Ultrafine Optoelectronic Systems, School of Materials Science & Engineering, Beijing Institute of Technology, 5 Zhongguancun South Street, Haidian District, Beijing, 100081, China
[e] Center for Electron Microscopy, TUT-FEI Joint Laboratory, Tianjin Key Laboratory of Advanced Functional Porous Materials, Institute for New Energy Materials & Low-Carbon Technologies, School of Materials Science and Engineering, Tianjin University of Technology, Tianjin, 300384, China
[f] Beijing Synchrotron Radiation Facility, Institute of High Energy Physics, Chinese Academy of Sciences, Beijing, 100049, China

ARTICLE INFO

Keywords:
Layered double hydroxides
Gradient materials
Electron transfer
Oxygen evolution

ABSTRACT

Breaking the symmetry in catalysts through interface engineering has emerged as a new dimension in enhancing the catalytic performances, while the long-range asymmetry (i.e. in nanometer scale) in catalysts can hardly be achieved by alloying or doping. Herein, we introduce asymmetrical gradient effect into NiFe layered double hydroxide (NiFe-LDH) at nano scale via a simple nanoarray construction strategy on Ni foam substrate. The electron energy loss spectroscopy, extended X-Ray absorption fine structure and other characterizations together revealed the concentration and valence states gradients in NiFe-LDH nanoarrays. Subsequently, the gradient effect leads to distinctly optimized binding strength of active sites to oxygen evolution intermediates, better electron transfers and boosted oxygen evolution performances, which are absent in non-gradient NiFe-LDH catalysts. Such long-range gradient effects in nanoarray materials provide new opportunities to understand their boosted catalytic performances and to rationally design better catalytic materials.

1. Introduction

Designing excellent oxygen evolution reaction (OER) catalysts is essential for the development of water splitting devices and rechargeable metal-air batteries [1,2]. Transition metal-based oxides/hydroxides, especially NiFe layered double hydroxides (NiFe-LDH), have been acknowledged as promising alternatives to noble metal based OER catalysts in alkaline media due to the high reactivity [3,4]. And a series of works have been emerged including composition tailoring [5], defects introduction [6] and single layer manipulating [7] to further improve their performances. It is generally recognized that the OER intrinsic properties are enhanced by optimizing the binding strength to oxygenated intermediates [8] and facilitating the electron transports [9] through varied approaches. However, most of these methods were based on uniform or homogeneous materials without asymmetric structures, which can indeed tailor the surface adsorption energy at local manipulated area but were not able to modulate the transportation directions of electrons or holes through the entire catalysts to endow further performance promotion [10,11].

Material gradients have shown great potential to facilitate the electron transportation [12], tailor the interfacial interactions [13] and coordination/electronic environment [14] in Li-ion battery [15], photocatalysis [16] and nanogenerator [17] etc. via “breaking the symmetry” strategy. Performances of materials can be manipulated by

* Corresponding author. State Key Laboratory of Chemical Resource Engineering, Beijing Advanced Innovation Center for Soft Matter Science and Engineering, Beijing University of Chemical Technology, Beijing, 100029, China.
** Corresponding author.
*** Corresponding author.
E-mail address: sunxm@mail.buct.edu.cn (X. Sun).
[1] These authors contribute equally to this work.

https://doi.org/10.1016/j.nanoen.2019.04.014
Received 16 February 2019; Received in revised form 20 March 2019; Accepted 3 April 2019
Available online 06 April 2019

modulating the extent of gradient, but most of the studies still suffer from limited transition boundary thickness (several atomic layers scale) [18]. How to maximize the gradient-induced asymmetrical coordination/electronic structures throughout the whole range of catalysts and at the same time maintain the structure robustness remains a challenge. Fortunately, the LDH laminates, in which the majority M^{2+} has a high compatibility to minority M^{3+}, with highly tunable composition and structure controlled by synthetic pH environment and feeding M^{2+}:M^{3+} ratio, seems to be a potential candidate to construct long-range gradient catalyst with structural stability [19].

Based on above concerns, NiFe-LDH grown on Ni foam prepared via one-step hydrothermal method was refocused. The existence of concentration and valance state gradients from bottom to top of nanoarrays were evidenced by TEM lines scan, Electron energy loss spectroscopy (EELS) and X-ray photoelectron spectroscopy (XPS). Such gradually stretched Ni-O/Fe-O bonds (vs. gradient-free $Ni_{3.5}Fe_1$-LDH) and as formed electron-rich $Ni^{2-\delta}$ and $Fe^{3-\delta}$ (partially reduced by Ni foam) jointly promote the OH* binding to Ni sites (in good agreement with the shifting of pseudocapacitive redox peaks), modulate *O and *OOH binding to Fe sites (in accord with the simulation results), which have been reported as the optimal pathway for OER on $NiFe(OOH)_x$. Furthermore, electrons transfer from top to the bottom and holes transfer vice versa are also favored by band structure change under the influence of the gradient. As a result, the prepared gradient Fe-doped NiFe-LDH on Ni foam illustrates OER onset over-potential as low as 180 mV with good stability at 50 mA/cm^2 for 24 h. The preparation and recognition of gradients in NiFe-LDH nanoarrays not only unveil their high intrinsic activity but also provide insights on developing other long-range gradient materials for energy conversion and storage.

2. Results and discussion

The Nanoarray-LDH were prepared by a simple hydrothermal method [20]. And the Colloidal-LDH nanosheets prepared by co-precipitation method was used as counterparts [21]. The elemental distribution and electronic structure comparisons of Colloidal-LDH and Nanoarray-LDH were studied by TEM line scan (Fig. 1a and Fig. S1) and electron energy loss spectroscopy (EELS) (Fig. 1c and Fig.S1). A uniform Ni:Fe ratio (3.42:1) can be found in Colloidal-LDH (Fig. S1), which is close to the feeding ratio. For comparison, Fig. 1a and b reveal the Fe-concentration gradient distribution from the bottom to the top in Nanoarray-LDH, in which the Ni:Fe ratio decreases from 3.5:1 to 2.4:1, corresponding to a Fe enrichment at the top of Nanoarray-LDH.

The valence of Fe in Colloidal-LDH has no obvious change from edge to center in Fig. S1 due to the single coordination environment (Fe^{3+}-O-Ni^{2+}) in uniform NiFe-LDH laminates. At the same time, the Ni EELS spectra of Colloidal-LDH can be fitted into two peaks, corresponding to a low valent Ni in Ni-O-Ni and a high valent Ni in Ni-O-Fe (high valence of Ni derived from the electron transfer between weak electronegativity Ni^{2+} with strong electronegativity Fe^{3+}). In contrast to the Colloidal-LDH, the valence states evolutions of Fe and Ni from bottom to top in Nanoarray-LDH are revealed to be very different (Fig. 1c). The overall valence states of both Ni and Fe from bottom to top in Nanoarray-LDH are lower than that in Colloidal-LDH due to the reducing effect by Ni foam. The Fe^{3+} is observed at the bottom of the Nanoarray-LDH in Fig. 1c as Fe^{3+} has low K_{sp} that would first nucleate on Ni foam with the increasing of pH value [22]. The negative shift of Fe energy loss in Nanoarray-LDH compared with typical Fe^{3+}-O can be attributed to the $Fe^{3-\delta}$-O (electron-rich Fe^{3+}, the formation of $Fe^{3-\delta}$ will be discussed in the following part). As for valence state of Ni in Fig. 1c, the high valence state corresponds to Ni^{2+}, while the low valence state was indexed to high concentration of $Ni^{2-\delta}$ (electron-rich Ni^{2+}) generated from Ni foam oxidation by Fe^{3+} and Ni^{2+} as well as Fe^{3+} nucleate during the urea hydrolysis (forming $Ni^{2-\delta}$-O-Ni^{2+}-O-Fe^{3+}). The afterwards nucleation of high K_{sp} $Ni^{2-\delta}$ and $Fe^{3-\delta}$ on top of Nanoarray-LDH at a high pH environment caused by further hydrolysis of urea results in $Ni^{2-\delta}$-O-$Fe^{3-\delta}$ moiety, which further lead to the lower valence state of top Ni in Nanoarray-LDH as compared with bottom Ni^{2+}.

Based on the TEM line scan and EELS characterizations, the growth mechanisms of Colloidal-LDH prepared by co-precipitation method and Nanoarray-LDH prepared by hydrothermal method are proposed in Scheme 1a and 1b. Ni^{2+} and Fe^{3+} will nucleate simultaneously in the preparation of Colloidal-LDH, forming gradient-free Colloidal-LDH. However, when Ni foam is presented as substrate, Fe^{3+} ions would first partially oxidize Ni foam surface prior to nucleation of LDH, thus there would be highly concentrated Ni^{2+} and $Ni^{2-\delta}$ ions close to Ni foam. In the nucleation process of LDH, Fe^{3+}, Ni^{2+} ions with low K_{sp} (1.1×10^{-36} and 5.48×10^{-16}, respectively) and part of high concentration $Ni^{2-\delta}$ would also nucleate on the surface of Ni foam, forming $Ni^{2-\delta}$-O-Ni^{2+}-O-Fe^{3+} moiety and leading to higher Ni:Fe ratio in NiFe-LDH attached to Ni foam. With further hydrolysis of urea, the pH of the synthetic environment goes up and further epitaxial growth of NiFe-LDH happens. In this stage, $Fe^{3-\delta}$ and $Ni^{2-\delta}$ with high K_{sp} would sediment together to form $Fe^{3-\delta}$-O-$Ni^{2-\delta}$-O-$Fe^{3-\delta}$ structure and the Ni:Fe ratio would decrease along the direction away from the Ni foam as substrate. To verify the proposed growth mechansim of NiFe-LDH by hydrothermal method, the pH values are monitored by every 2 h. As shown in Fig. S2, the pH values climb sharply with elevated temperature due to the hydrolysis of urea, and then increase gently due to the coordination between metal cations with OH^-. In summary, growing concentration of Fe along with increasing electron density of both Ni and Fe from the bottom to the top of NiFe-LDH formed during the growth of arrayed LDH on Ni foam, as can be confirmed by the TEM, SEM line scan and EELS spectra characterizations, indicating a gradient structure. Furthermore, the increasing electron density in Nanoarray-LDH may well-resolved the higher concentration of unpaired electron in

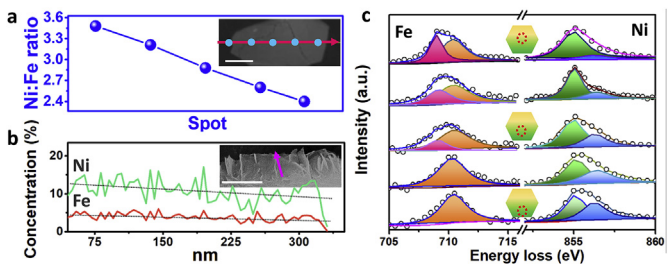

Fig. 1. Analysis of chemical and electronic structure. (**a**) TEM line scan, (**b**) SEM line scan, (**c**) EELS spectra of Fe-L edge and Ni-L edge in Nanoarray-LDH. Inserts are the corresponding TEM and SEM images. Bar in (a) stands for 100 nm, bar in (b) stands for 500 nm.

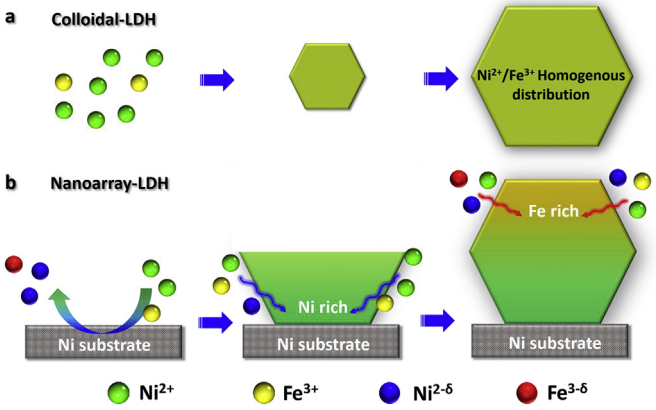

Scheme 1. Illustration of the growth of (**a**) Colloidal -LDH prepared by co-precipitation method and (**b**) Nanoarray-LDH prepared by hydrothermal method.

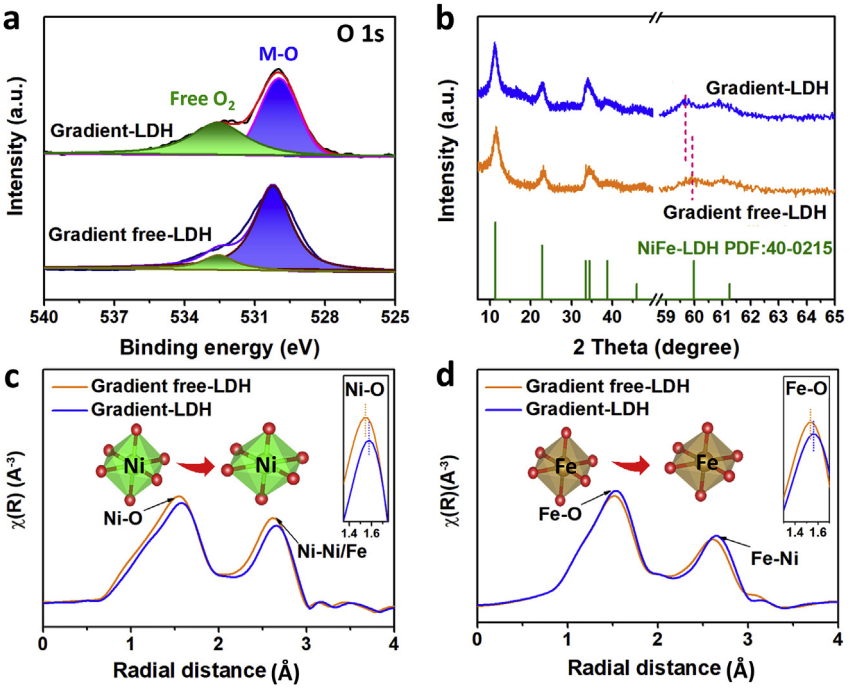

Fig. 2. Comparison of (**a**) XPS spectra, (**b**) XRD pattern, (**c**) & (**d**) Fourier transform magnitudes of EXAFS data for the Ni and Fe in NiFe-LDH with/without gradient composition.

it (Fig. S3). In the following discussions, the Nanoarray-LDH is named as gradient-LDH while Colloidal-LDH is denoted as gradient-free-LDH.

The morphology of NiFe-LDH with/without gradient structure was revealed by TEM in Fig. S4 and SEM in Fig. S5, no obvious microcracks or lattice distortion can be observed in gradient NiFe-LDH nanosheets, indicating that gradient Fe doping has little impact on the morphology and structure of NiFe-LDH due to isomorphs substitution of Ni^{2+} and Fe^{3+} by $Ni^{2-\delta}$ and $Fe^{3-\delta}$.

In Fig. 2a, the binding strength of NiFe-LDH with/without gradient composition to oxygenated intermediates is revealed by X-ray photoelectron spectroscopy (XPS) O 1s spectra. The O species at 529.8 eV are assignable to the typical metal-oxygen (M − O) bonds in NiFe-LDH. The O species at 532.8 eV can be ascribed to adsorbed free O-O bonds at the materials' surface [23]. The intensity and binding energy of M − O bonds in NiFe-LDH have negligible changes before and after gradient Fe doping. However, there observes an obvious increase in intensity of adsorbed O-O in NiFe-LDH after gradient Fe doping, suggesting enhanced binding strength of gradient NiFe-LDH surface to oxygenated intermediates [8]. The gradient-LDH has diffraction peaks corresponding to typical NiFe-LDH structure (JCPDS 40–0215), which is similar to the gradient free NiFe-LDH. The detailed XRD patterns in Fig. 2b, where (110) diffraction peak of gradient NiFe-LDH shifts to lower angle compared to the gradient-free counterpart, indicating stretched metal-oxygen-metal (M-O-M) bond along with electron-rich structure of both Ni and Fe in gradient NiFe-LDH (Fig. S6) [24]. In Fig. 2c and d, bond length evolution of NiFe-LDH with/without gradient composition was studied and a stretched Ni-O/Fe-O bond can be found in gradient NiFe-LDH by Fourier transformed magnitudes extended X-ray absorption fine structure (EXAFS) spectra, indicating higher covalency of the M − O bond in NiFe-LDH induced by gradient Fe doping. Furthermore, the XPS results of gradient NiFe-LDH in Fig. 2a are consistent to the *d* band theory and the tension in gradient NiFe-LDH, where tension in metal oxides/hydroxides can normally enhance binding strength to oxygenated intermediates (in this case, the stronger binding of gradient NiFe-LDH surface to free O-O) [25,26].

To ensure the two samples have the same "loading states" on Ni foam, gradient NiFe-LDH nanosheets were reloaded on fresh Ni foam for electrochemical characterization for comparison with gradient free-LDH to eliminate the influence from the substrates. Furthermore, those two nanosheets were checked in surface area and the electrochemical surface area (ECSA) (Table. S1 and Fig. S7).

BET and iR-corrected OER performances of NiFe-LDH (gradient- v.s. gradient free) were studied in Fig. 3, and ECSA-correct OER perperformances was shown in Fig.S8. As shown in Fig. 3a, OER onset potential of gradient-LDH is as low as 1.41 V (vs. RHE), which is ~40 mV lower than that of gradient free-LDH, illustrating its higher intrinsic activity. At the same time, turnover frequency (TOF) of gradient-LDH is 0.22 s^{-1}, which is ~30% higher than that of gradient free-LDH (0.17 s^{-1}). The Ni oxidation peak position can be used to investigate the OH^- binding to catalysts surface, which is not the same but positively correlated to the first step of OER (formation of *OH on NiFe-LDH). In Fig. 3a, the Ni oxidation peak in gradient-LDH appears at 1.32 V, around 15 mV earlier than the counterpart, indicating the stronger binding of gradient-LDH to OH^- in electrolyte [27]. The two reduction peaks from Ni^{3+} to Ni^{2+} may attribute to the different coordination of Ni (Ni-O-Ni or Ni-O-Fe) in NiFe-LDH. Tafel slopes in Fig. 3b show similar OER kinetics on both gradient- and gradient free-LDH, but charge transfer resistance (R_{ct}) of different samples studied by Nyquist plots in Fig. 3c shows that electron transfer can be facilitated in gradient-LDH nanoarray compared with that of gradient free-LDH. We ascribe this facilitated electron transfer to the gradient composition and valence states in gradient-LDH (will be discussed later). The similar system resistance (R_s) for both samples indicates the tight interaction between NiFe-LDH nanosheets with substrate Ni foam. Laviron analysis in Fig. 3d and Fig.S9 further verifies the higher redox constant (K_s) and stronger binding of gradient-LDH to OH^- [28,29], and the gradient-LDH shows satisfying electrochemical stability at 50 mA/cm^2 for 24 hrs as shown in Fig. S10.

As revealed in Fig. 1c where part of Fe^{3+} has transformed into electron-rich $Fe^{3-\delta}$ in gradient NiFe-LDH (Fig. S5), and $Fe^{3-\delta}$ has already shown its positive effect in tailoring OER activity of NiFe-LDH [30], then NiFe-LDH with decreasing Ni:Fe ratio and a small portion of Fe^{2+} in it was prepared (gradient-free $Ni_{3.5}Fe_{1.0}{}^{3+}$-LDH, $Ni_{3.0}Fe_{0.25}{}^{2+}Fe_{0.75}{}^{3+}$-LDH and $Ni_{2.5}Fe_{0.5}{}^{2+}Fe_{0.5}{}^{3+}$-LDH) to compare its

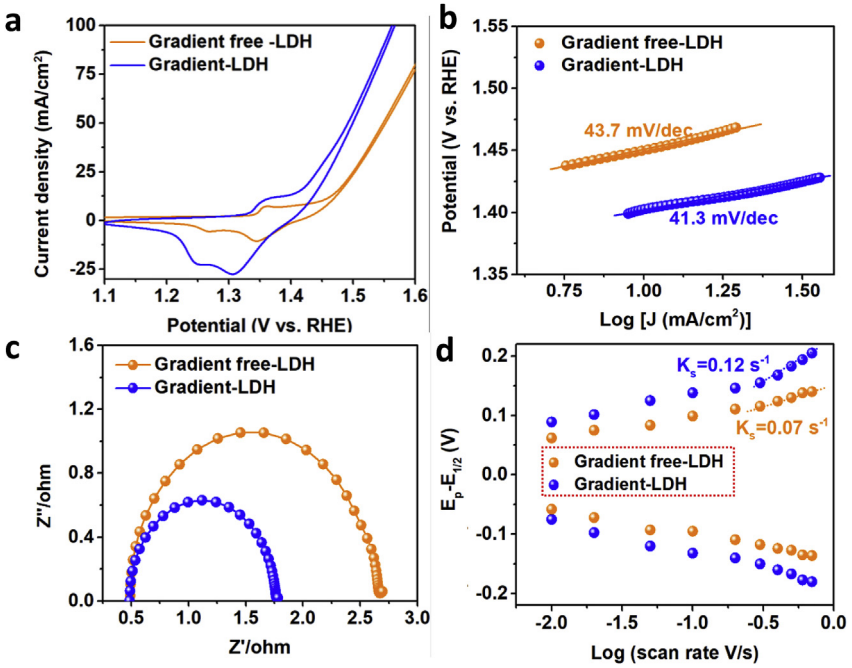

Fig. 3. (**a**) Polarization curves (after BET & iR-correction), (**b**) Tafel slopes derived from polarization curves, (**c**) Nyquist plots, (**d**) Laviron analysis of NiFe-LDH with/without gradient composition.

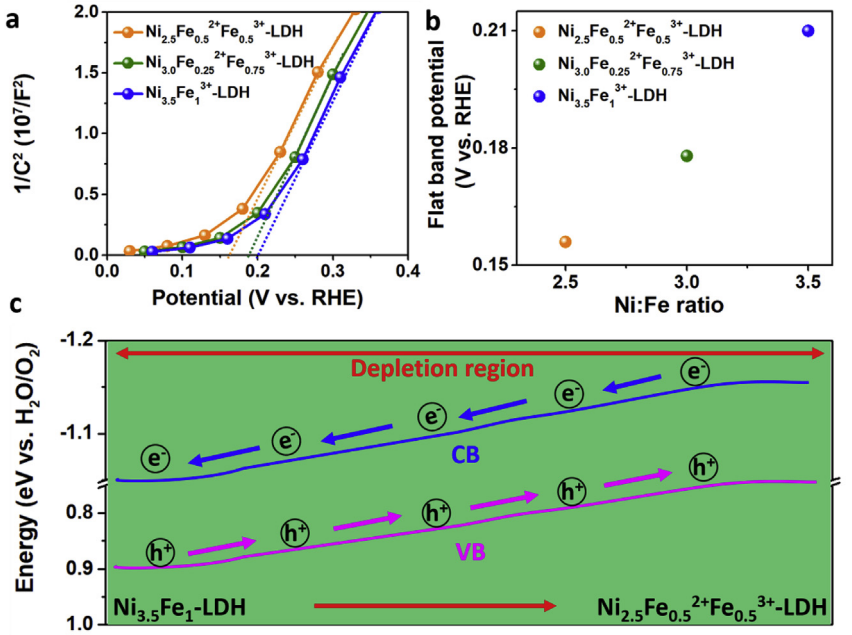

Fig. 4. (**a**) Mott-Schottky plots of NiFe-LDH with various Ni:Fe ratios and Fe^{2+} concentration. (**b**) Flat-band potentials of NiFe-LDH with various Ni:Fe ratios and Fe^{2+} concentration derived from Mott-Schottky plots. (**c**) Electron transfer illustration in gradient NiFe-LDH.

performance with gradient NiFe-LDH (the $Ni^{2-\delta}$ is supposed to be considered here, however we can hardly prepare NiFe-LDH with tunable concentration of $Ni^{2-\delta}$ in it). In Fig. S11, the gradient NiFe-LDH on glassy carbon electrode still shows the best OER activity even comparing with gradient-free $Ni_{3.0}Fe_{0.25}{}^{2+}$ $Fe_{0.75}{}^{3+}$-LDH with the same Ni:Fe ratio. If the OER activity of gradient NiFe-LDH is merely related to the metal-oxygen bond length, Ni:Fe ratio and valence states of active sites, the OER performance of gradient NiFe-LDH with overall Ni:Fe = 3:1 should somehow locate between the gradient-free $Ni_{2.5}Fe_{0.5}{}^{2+}$ $Fe_{0.5}{}^{3+}$-LDH and $Ni_{3.5}Fe_{1.0}{}^{3+}$-LDH (hypothetical result in Fig. S12). However, the low onset potential and fast current density increase of gradient NiFe-LDH (practical result in Fig. S12) indicate that another indispensable contribution apart from the enhanced binding strength to intermediates would benefit its intrinsic OER activity. By further investigating band structure of NiFe-LDH with different Ni:Fe ratios and concentration of Fe^{2+}, we propose that this extra part of contribution comes from the favorable electron transfer trend induced by gradient doping in NiFe-LDH.

The electron transfer trends in gradient NiFe-LDH were studied by characterizing the position of conduction band minimum (CBM) and valence band maximum (VBM) positions of gradient-free $Ni_{3.5}Fe_{1.0}{}^{3+}$-LDH, $Ni_{3.0}Fe_{0.25}{}^{2+}Fe_{0.75}{}^{3+}$-LDH and $Ni_{2.5}Fe_{0.5}{}^{2+}Fe_{0.5}{}^{3+}$-LDH,

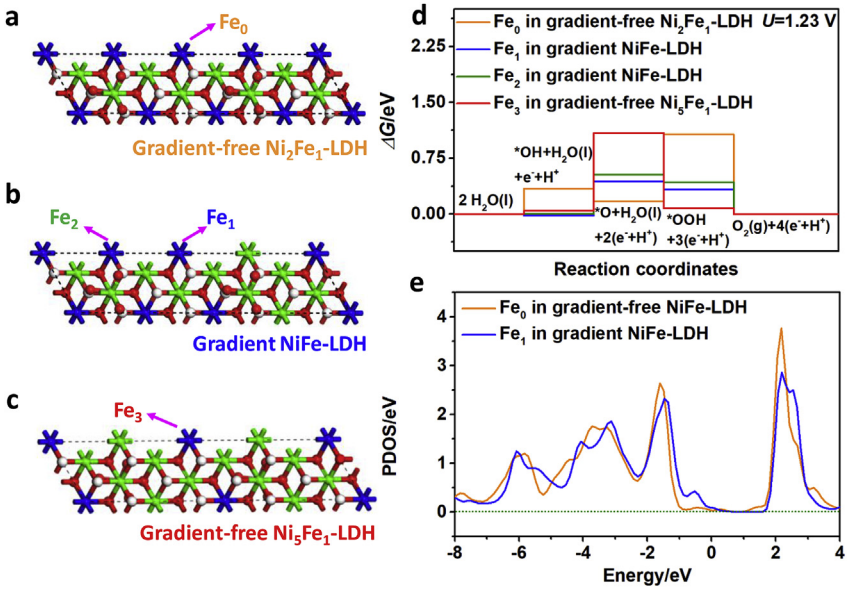

Fig. 5. Schematic illustration of NiFe-LDH with/without gradient composition. (**a**) Fe_0 in gradient-free Ni_2Fe_1-LDH was chosen as the active site. (**b**) Fe_1 and Fe_2 in gradient NiFe-LDH were chosen as active sites, respectively. (**c**) Fe_3 in gradient-free Ni_5Fe_1-LDH was chosen as the active site. (**d**) Theoretical calculations of OER catalysis on different Fe sites in NiFe-LDH without/with gradient composition. (**e**) Partial density of states (PDOS) of Fe_0 and Fe_1.

respectively. The CBM and VBM of gradient-free $Ni_{3\cdot5}Fe_{1.0}{}^{3+}$-LDH, $Ni_{3\cdot0}Fe_{0.25}{}^{2+}Fe_{0.75}{}^{3+}$-LDH and $Ni_{2\cdot5}Fe_{0.5}{}^{2+}Fe_{0.5}{}^{3+}$-LDH were collectively characterized by valence band XPS spectra (Fig. S13) and UV–vis (Fig. S14 and Tab. S2) as (−1.13 eV, 0.91 eV), (−1.14 eV, 0.83 eV) and (−1.16 eV, 0.73 eV) (vs. H_2O/O_2), respectively. In Fig. 4a and b, the Mott-Schottky plots reveal the flat band potential (vs. RHE, pH = 13.6) of gradient-free $Ni_{3\cdot5}Fe_{1.0}{}^{3+}$-LDH, $Ni_{3\cdot0}Fe_{0.25}{}^{2+}Fe_{0.75}{}^{3+}$-LDH and $Ni_{2\cdot5}Fe_{0.5}{}^{2+}Fe_{0.5}{}^{3+}$-LDH. The results are positively correlated to the data revealed by XPS and UV–vis. Since the CBM of gradient-free $Ni_{2\cdot5}Fe_{0.5}{}^{2+}Fe_{0.5}{}^{3+}$-LDH (−1.16 V) is more negative than that of gradient-free $Ni_{3\cdot5}Fe_{1.0}{}^{3+}$-LDH (−1.13 V), the electron would transfer smoothly and efficiently from CBM of $Ni_{2\cdot5}Fe_{0.5}{}^{2+}Fe_{0.5}{}^{3+}$-LDH to the CBM of $Ni_{3\cdot5}Fe_{1.0}{}^{3+}$-LDH as schematically shown in Fig. 4c. So it is reasonable to deduce that the electrons would also transfer from the top to the bottom of gradient NiFe-LDH nanosheets by gradient doping effect [31–34]. Furthermore, the depletion region (DR) distributing throughout the gradient NiFe-LDH indicate the kinetically facilitated electron transfer. The four steps of oxygen evolution reaction in alkaline media involve the continuous adsorption of OH^- on the active sites by transferring electrons away from the active sites to glassy carbon electrode surface and holes vice versa, thus the favorable holes transfer from bottom to top in gradient NiFe-LDH will facilitate the OH^- oxidation and deprotonating step on the top active sites, and suppress undesired backward or spontaneously chaotic electron transduction in NiFe-LDH [35], which would lead to facilitated OER kinetics of gradient NiFe-LDH.

To highlight the gradient doping effect on OER catalysis of NiFe-LDH, we constructed three models in Fig. 5a-**5c** to calculate the OER free energy of NiFe-LDH without/with gradient composition. The free energy evolution in Fig. 5d shows that Fe sites in gradient NiFe-LDH have a stronger binding strength to the OH^- in OER (lower adsorption energy in first step) and modulated ΔG_{O^*} (RDS) compared to the gradient-free NiFe-LDH, which can reasonably lead to lower theoretical OER onset potential and in good agreement to the experimental results as displayed in Fig. 3a. Furthermore, the PDOS of Fe_0 in gradient-free NiFe-LDH and Fe_1 in gradient NiFe-LDH were studied in Fig. 5e. The upshift of valence band maximum (VBM) of Fe_2 reveals the increasing electron density (in line with EELS and XPS), which enhances adsorption of gradient NiFe-LDH to OER intermediates according to the *d* band theory [26,36].

To highlight the universal effect of gradient in NiFe-LDH nanoarray, we further prepare NiFe-LDH nanoarray with other Ni:Fe ratios as shown in Fig.S15 and Fig.S16. The structure of NiFe-LDH nanoarray and the corresponding OER performances conclusively confirm the positive effect of gradient on the water Oxidation activity of NiFe-LDH nanoarray.

3. Conclusion

Breaking the symmetry by introduction of gradients has great potential to further boost the performances of electrocatalysts, while long-range gradient in nanomaterials can hardly be obtained by a simple and facile method. Here we prepare concentration and valence states gradients in NiFe-LDH nanaoarray by a simple hydrothermal synthesis on a Ni substrate, on which partially oxidized $Ni^{2-\delta}$ and partially reduced $Fe^{3-\delta}$ formed. Detailed characterizations including EELS, EXAFS and XPS suggest that the long-range gradient in NiFe-LDH contributes to its improved oxygen evolution performance by enhancing its binding strength to oxygenated intermediates and facilitating the favorable electron transfer. Such concentration and valence states gradient of metal ions in nanoarray materials provide new insights to understand their boosted catalytic performances and to rationally design better catalytic materials.

Acknowledgements

This work was financially supported by the National Natural Science Foundation of China, the Program for Changjiang Scholars and Innovative Research Team in the University, the Fundamental Research Funds for the Central Universities, the Long-Term Subsidy Mechanism from the Ministry of Finance and the Ministry of Education of China, the National Key Research and Development Project, the Singapore Ministry of Education Academic Research Fund (AcRF) Tier 1: RG10/16, RG9/17, RG115/17; Tier 2: MOE2016-T2-2-004, and the Nanyang Technological University internal funding.

Appendix A. Supplementary data

Supplementary data to this article can be found online at https://doi.org/10.1016/j.nanoen.2019.04.014.

References

[1] D.A. Kuznetsov, B. Han, Y. Yu, R.R. Rao, J. Hwang, Y. Román-Leshkov, Y. Shao-Horn, Joule 2 (2018) 225–244.
[2] F. Song, L. Bai, A. Moysiadou, S. Lee, C. Hu, L. Liardet, X. Hu, J. Am. Chem. Soc. 140

(2018) 7748–7759.
[3] F. Dionigi, P. Strasser, Adv. Energy Mater. 6 (2016) 1600621.
[4] M. Gong, Y. Li, H. Wang, Y. Liang, J.Z. Wu, J. Zhou, J. Wang, T. Regier, F. Wei, H. Dai, J. Am. Chem. Soc. 135 (2013) 8452–84555.
[5] K. Fan, H. Chen, Y. Ji, H. Huang, P.M. Claesson, Q. Daniel, B. Philippe, H. Rensmo, F. Li, Y. Luo, L. Sun, Nat. Commun. 7 (2016) 11981.
[6] R. Liu, Y. Wang, D. Liu, Y. Zou, S. Wang, Adv. Mater. 29 (2017) 1701546.
[7] F. Song, X. Hu, Nat. Commun. 5 (2014) 4477.
[8] H.B. Tao, L. Fang, J. Chen, H.B. Yang, J. Gao, J. Miao, S. Chen, B. Liu, J. Am. Chem. Soc. 138 (2016) 9978–9985.
[9] Z. Lu, W. Xu, W. Zhu, Q. Yang, X. Lei, J. Liu, Y. Li, X. Sun, X. Duan, Chem. Commun. 50 (2014) 6479–6482.
[10] D. Xu, M.B. Stevens, Y. Rui, G. DeLuca, S.W. Boettcher, E. Reichmanis, Y. Li, Q. Zhang, H. Wang, Electrochim. Acta 265 (2018) 10–18.
[11] N. Han, F. Zhao, Y. Li, J. Mater. Chem. 3 (2015) 16348–16353.
[12] T. Liu, A. Li, C. Wang, W. Zhou, S. Liu, L. Guo, Adv. Mater. 30 (2018) 1803590.
[13] Y. Heo, S. Choi, J. Bak, H.-S. Kim, H.B. Bae, S.-Y. Chung, Adv. Energy Mater. 8 (2018) 1802481.
[14] Z. Xi, J. Li, D. Su, M. Muzzio, C. Yu, Q. Li, S. Sun, J. Am. Chem. Soc. 139 (2017) 15191–15196.
[15] J. Kim, H. Cho, H.Y. Jeong, H. Ma, J. Lee, J. Hwang, M. Park, J. Cho, Adv. Energy Mater. 7 (2017) 1602559.
[16] Z. Luo, C. Li, S. Liu, T. Wang, J. Gong, Chem. Sci. 8 (2017) 91–100.
[17] X. Nie, B. Ji, N. Chen, Y. Liang, Q. Han, L. Qu, Nanomater. Energy 46 (2018) 297–304.
[18] J. Tang, H. Sheng, Z. Li, H. Shen, L. Zhao, H. Zhong, J. Phys. Chem. C 122 (2018) 4583–4588.
[19] M. Xu, M. Wei, Adv. Funct. Mater. 28 (2018) 1802943.
[20] Z. Lu, L. Qian, Y. Tian, Y. Li, X. Sun, X. Duan, Chem. Commun. 52 (2016) 908–911.
[21] D. Zhou, Z. Cai, Y. Bi, W. Tian, M. Luo, Q. Zhang, Q. Xie, J. Wang, Y. Li, Y. Kuang, X. Duan, M. Bajdich, S. Siahrostami, X. Sun, Nano Res 11 (2018) 1358–1368.
[22] S. Anantharaj, K. Karthick, S. Kundu, Mater. Today Energy 6 (2017) 1–26.
[23] L. Xu, Q. Jiang, Z. Xiao, X. Li, J. Huo, S. Wang, L. Dai, Angew. Chem. Int. Ed. 55 (2016) 5277–5281.
[24] D. Zhou, S. Wang, Y. Jia, X. Xiong, H. Yang, S. Liu, J. Tang, J. Zhang, D. Liu, L. Zheng, Angew. Chem. Int. Ed. 131 (2019) 746–750.
[25] J.K. Nørskov, T. Bligaard, A. Logadottir, S. Bahn, L.B. Hansen, M. Bollinger, H. Bengaard, B. Hammer, Z. Sljivancanin, M. Mavrikakis, Y. Xu, S. Dahl, C.J.H. Jacobsen, J. Catal. 209 (2002) 275–278.
[26] J. Rossmeisl, A. Logadottir, J.K. Nørskov, Chem. Phys. 319 (2005) 178–184.
[27] D. Zhou, Y. Jia, H. Yang, W. Xu, K. Sun, J. Zhang, S. Wang, Y. Kuang, B. Liu, X. Sun, J. Mater. Chem. 6 (2018) 21162–21166.
[28] E. Laviron, J. Electroanal. Chem. 101 (1979) 19–28.
[29] J. Wang, L. Gan, W. Zhang, Y. Peng, H. Yu, Q. Yan, X. Xia, X. Wang, Sci. Adv. 4 (2018) eaap7970.
[30] Z. Cai, D. Zhou, M. Wang, S. Bak, Y. Wu, Z. Wu, Y. Tian, X. Xiong, Y. Li, W. Liu, S. Siahrostami, Y. Kuang, X.-Q. Yang, H. Duan, Z. Feng, H. Wang, X. Sun, Angew. Chem. Int. Ed. (2018) 9392–9396.
[31] H. Wu, Z. Kang, Z. Zhang, Z. Zhang, H. Si, Q. Liao, S. Zhang, J. Wu, X. Zhang, Y. Zhang, Adv. Funct. Mater. 28 (2018) 1802015.
[32] Y. Liang, Y. Yu, Y. Huang, Y. Shi, B. Zhang, J. Mater. Chem. 5 (2017) 13336–13340.
[33] X.Q. Tian, X.R. Wang, Y.D. Wei, L. Liu, Z.R. Gong, J. Gu, Y. Du, B.I. Yakobson, Nano Lett. 17 (2017) 7995–8004.
[34] Q. Gong, Y. Wang, Q. Hu, J. Zhou, R. Feng, P.N. Duchesne, P. Zhang, F. Chen, N. Han, Y. Li, Nat. Commun. 7 (2016) 13216.
[35] M. Krzeszewski, E.M. Espinoza, C. Cervinka, J.B. Derr, J.A. Clark, D. Borchardt, G.J.O. Beran, D.T. Gryko, V.I. Vullev, Angew. Chem. Int. Ed. 57 (2018) 12365–12369.
[36] J. Greeley, I.E. Stephens, A.S. Bondarenko, T.P. Johansson, H.A. Hansen, T.F. Jaramillo, J. Rossmeisl, I. Chorkendorff, J.K. Norskov, Nat. Chem. 1 (2009) 552–556.